Analyst

PAPER

View Article Online
View Journal | View Issue

Cite this: *Analyst*, 2022, **147**, 1367

Nanoclay-based sensor composites for the facile detection of molecular antioxidants†

Adél Szerlauth,[a,b] Lilla Szalma,[b] Szabolcs Muráth,[a,b] Szilárd Sáringer,[a,b] Gábor Varga,[b] Li Li[c] and István Szilágyi*[a,b]

The detection and quantification of antioxidant molecules is an important task in food science, the fine chemical industry and healthcare. Antioxidants help in preventing the deterioration of nutrition and healthcare products, while eliminating over-the-limit exogenic reactive species, which may lead to illnesses. In our contribution, an inexpensive and rapid method to determine the concentration of various molecular antioxidants was developed. The principle of the analysis relies on the cupric ion reducing antioxidant capacity (CuPRAC) method, which is based on the color-changing reduction of chelated Cu^{2+} ions. This complex was successfully immobilized on an alginate-functionalized layered double hydroxide (dLDH) nanosheet *via* electrostatic interactions. The synthesis conditions of alginate (NaAlg) and the cupric complex were optimized, and the optimized composite was fabricated on cellulose paper to obtain a sensing platform. The paper-based sensor was superior to the ones prepared without the dLDH support, as the limit of detection (LOD) values decreased, and the linearity ranges broadened. The results offer a single-point measurement to evaluate the antioxidant efficiency in a cuvette-based method. The superior ability of the sensor was assigned to the presence of solid dLDH particles, as they offer adsorption sites for the dissolved antioxidant molecules, which contributes significantly to the decrease of the diffusion limitation during the detection process.

Received 28th December 2021,
Accepted 19th February 2022

DOI: 10.1039/d1an02352g

rsc.li/analyst

Introduction

Antioxidants play an important role in protecting against unstable reactive substances generated during normal biochemical reactions, as they inhibit or reduce the harmful effects of reactive oxygen/nitrogen species (ROS/RNS), thus preventing the development of oxidative stress.[1–3] Enzymatic antioxidants (*i.e.*, superoxide dismutase, catalase, horseradish peroxidase) are essential for biochemical processes, where ROS is converted to H_2O_2 and ultimately to water. Next to the enzymatic species, the application of molecular antioxidants turned out to be a widely investigated area in the last decade.[4–6] Molecular antioxidants can be found in plants and in the human body as well, but synthetic representatives are also known.[7,8] Immobilization in/on various nanoparticles is a common tool to enhance the sensitivity (against pH, light, pressure, temperature, ionic strength, *etc.*) of both enzymatic and non-enzymatic substances, which can facilitate biomedical and industrial applications.[9–13] In the past decades, antioxidants have played an important role in fundamental sciences and in more applied disciplines and hence, assessment of antioxidant activity in different environments has become an extensively studied area.[14–17]

Accordingly, different methods were reported for measuring the antioxidant activity in pharmaceuticals, foods, or natural products. The classical color change-based techniques evaluate the antioxidant activity of different compounds or products by using a spectrophotometer. For instance, the 2,2-diphenyl-1-picrylhydrazyl (DPPH) assay is a conventional test to estimate the effectiveness of various antioxidants.[18] This test relies on the reduction of DPPH radicals and it is designed to determine the efficient concentration (EC_{50}), the antioxidant dose required to decrease the initial radical concentration to half. The Ferric Reducing Antioxidant Power (FRAP) assay was developed for the reduction of Fe^{3+} to Fe^{2+} ions[19] and the corresponding development of blue colored solutions, while decolorization of 2,2′-azinobis-(3-ethylbenzothiazoline-6-sulfonic acid) (ABTS) is also a common solution chemistry method to detect molecular antioxidants.[20] Besides, the Cu^{2+}-Neocuproine (Nc) complex has proven as a powerful tool to determine the antioxidant activity of different samples (so-called CuPRAC

[a]*MTA-SZTE Lendület Biocolloids Research Group, University of Szeged, H-6720 Szeged, Hungary. E-mail: szistvan@chem.u-szeged.hu*
[b]*Department of Physical Chemistry and Materials Science, University of Szeged, H-6720 Szeged, Hungary*
[c]*Australian Institute for Bioengineering and Nanotechnology, The University of Queensland, Brisbane, QLD-4072, Australia*

†Electronic supplementary information (ESI) available. See DOI: 10.1039/d1an02352g

assay).[21] During the test, Cu^{2+} ions are reduced to Cu^{+} followed by a color change, from light blue to orange. Such a color change allows spectrophotometric detection and determination of Trolox Equivalent Antioxidant Capacity (TEAC) values.

Since the above classical techniques applied in homogeneous solutions are sufficiently elaborated, numerous studies were concerned with the development of antioxidant sensing devices. The sensors reported in the literature to date are based on a color change[22,23] or operate on an electrochemical basis[15,24,25] and often involve nanomaterials[26–28] to quantify the antioxidant contents. For instance, immobilization of the $Cu(Nc)_2$ complex on membranes,[16] electrodes[17] or paper[29] led to the development of sensing elements, which are potential candidates for use in complex devices. Despite the good number of studies, the reported sensors still have limitations (*e.g.*, elevated limit of detection (LOD), lack of signal linearity or instability of the sensing composite under harsher environmental conditions), indicating the need for further investigations in the area of antioxidant sensors, similar to the efficient sensing elements developed in other fields.[30–33]

In the present work, the fabrication of a highly sensitive, paper-based colorimetric antioxidant sensor by functionalization of delaminated layered double hydroxide (dLDH) nanosheets was aimed. Conventional LDHs consist of positively charged metal hydroxide layers and charge compensating interlayer anions, however, their delamination into dLDHs provides a great tool to obtain unilamellar nanosheets with advanced features, such as biocompatibility, high specific surface area and anion exchange capacity.[34–37] Moreover, LDHs have already demonstrated their potential in the fabrication of various sensors.[38–41] An an anionic polyelectrolyte, sodium alginate (NaAlg) was applied to control the surface charge of dLDH particles, while the antioxidant sensing nature was achieved by functionalization of the polyelectrolyte coated nanosheets with the $Cu(Nc)_2$ complex. The structure and composition of the obtained sensing composite were explored by microscopy, spectroscopy and light scattering techniques. Antioxidant tests were first performed in dispersions using spectrophotometry and an image processing program after the formulation of the composite on cellulose filter paper. The sensing parameters such as linear range, LOD and TEAC values were determined for numerous molecular antioxidants.

Materials and methods

Materials

Magnesium nitrate hexahydrate ($Mg(NO_3)_2{\cdot}6H_2O$), aluminum nitrate nonahydrate ($Al(NO_3)_3{\cdot}6H_2O$), sodium hydroxide (NaOH) and lactic acid (85%) were purchased from Merck and used without purification. Copper(II) chloride dihydrate ($CuCl_2{\cdot}2H_2O$), neocuproine (Nc), trolox, L(+)-ascorbic acid, eugenol, diosmin, gallic acid, glutathione (reduced), catechin hydrate, tannic acid, chlorogenic acid (predominantly trans), sodium salicylate, sodium alginate (NaAlg), sodium chloride (NaCl) and ethanol were obtained from VWR International in analytical grade and used as received. For sensor preparation, cellulose filter paper (Whatman Grade 602H, VWR) and crayon were used. Ultrapure water was obtained from a Puranity TU3+ UV/UF system.

Preparation of dLDH nanosheets

A dLDH dispersion of 15 g L^{-1} concentration was prepared using the co-precipitation method as described elsewhere with some modifications.[42] Briefly, a 25 mL lactic solution containing lactic acid (40.0 mmol) and NaOH (64.0 mmol) was prepared. A 15 mL salt solution containing 8.0 mmol of $Mg(NO_3)_2$ and 4.0 mmol of $Al(NO_3)_3$ was quickly added to the lactic solution with continuous stirring for two hours, followed by sonication for 30 minutes. dLDH nanosheets were obtained after washing three times with distilled water *via* centrifugation and re-dispersed in deionized water. The size, charge, and morphology of dLDH nanosheets were characterized by dynamic light scattering (DLS) and transmission electron microscopy (TEM). For the latter measurements, a JEM-3010 ZEOL device at an acceleration voltage of 100 kV was used.

Light scattering methods

Electrophoretic and DLS measurements were carried out with a Litesizer 500 (Anton Paar) instrument. The device is equipped with a 40 mW laser source operating at 658 nm wavelength. The measurements were carried out in backscattering mode at 175° scattering angle.

For the determination of electrophoretic mobilities (μ), Ω-shaped plastic cuvettes were purchased from Anton Paar. The total sample volume for the experiments was 400 μL. During sample preparation, calculated amounts of NaAlg and dLDH dispersion were mixed to achieve the appropriate polyelectrolyte dose. To adsorb the copper complex on the polyelectrolyte coated particles, $Cu(Nc)_2$ solution, in calculated volume, was added to the particle dispersions. The mixtures were prepared one day before the measurements. 1 mM NaCl was used as the background electrolyte, the pH was set to 9 and the final particle concentration was 10 mg L^{-1}. Zeta potentials (ζ) were calculated using Smoluchowski's equation:[43]

$$\mu = \frac{\varepsilon\varepsilon_0\zeta}{\eta} \quad (1)$$

where ε is the relative permittivity of water, ε_0 is the permittivity of vacuum and η is the dynamic viscosity.

DLS measurements were carried out in disposable polystyrene cuvettes (VWR International). The final volume was 2 mL, and the sample preparation was the same as the one described for the electrophoretic measurements. Nevertheless, the DLS analyses were performed immediately after mixing the components to assess the initial stage of aggregation. To determine the particle size, the second cumulant fit was applied to the correlation function and the hydrodynamic radius (R_h) was calculated using the Einstein–Stokes equation:[44]

$$R_h = \frac{k_B T}{6\pi\eta D} \quad (2)$$

where k_B is the Boltzmann constant, T is the temperature and D is the translational diffusion coefficient. The stability ratio (W) values were used to express the speed of particle aggregation as follows:[45]

$$W = \frac{k_{fast}}{k} \quad (3)$$

where k is the apparent aggregation rate constant calculated from the increase in the hydrodynamic radius in time resolved DLS measurements and k_{fast} was determined during diffusion limited particle aggregation achieved in 1 M NaCl concentration. Further experimental details on W assessment are given elsewhere.[46]

Antioxidant test

The CuPRAC assay based on the reduction of the $Cu(Nc)_2$ complex was applied to measure the antioxidant activity (Scheme S1 in the ESI†).[47] From the molecular antioxidants (trolox, sodium salicylate, diosmin, glutathione, ascorbic acid, chlorogenic acid, catechin, eugenol, gallic acid and tannic acid), 1 mM aqueous solutions were prepared, while $CuCl_2{\cdot}2H_2O$ and Nc were dissolved in a 50 v% ethanol–water mixture to reach 1 mM complex concentration and 1 : 1 metal-to-ligand ratio. The total reaction mixture was 2 mL. During the measurements, the complex concentration was set to 0.1 mM, while the antioxidant concentration was systematically varied. The concentration of the sensing composites in the cuvette was set to 10 mg L^{-1}. After 30 minutes of reaction time, the absorbance was measured at 450 nm wavelength. To determine the TEAC values, the molar absorbance (ε) values of the antioxidants and trolox (reference molecule) were compared:[13]

$$\mathrm{TEAC} = \frac{\varepsilon_{AO}}{\varepsilon_{Trolox}}. \quad (4)$$

Sensor fabrication and analysis

To prepare paper-based sensors, a conventional crayon was used to draw the desired pattern on both sides of filter paper. Thereafter, the filter paper was placed in an oven and heated at 150 °C for 5 minutes. To measure the antioxidant activity, 100 μL of $Cu(Nc)_2$ or immobilized $Cu(Nc)_2$ was dropped on the surface of the filter paper. After drying, 20 μL of antioxidant solution was added at different concentrations. The sensors were allowed to air-dry at room temperature for 30 minutes and scanned using a Kyocera ECOSYS M5526cdn scanner with a resolution of 1200 dots per inch. The color intensity was analyzed using the ImageJ software in the RGB color range. Since the sensors turned to an orange color after the addition of the antioxidant, blue, as the complementary color, was used to calculate the change in intensity during the analysis. The ΔMBV values were determined using the following equation:

$$\Delta\mathrm{MBV} = \mathrm{MBV}_{control} - \mathrm{MBV}_{AO} \quad (5)$$

where $MBV_{control}$ is the measured mean blue value of the control (without antioxidant) and MBV_{AO} is the measured mean blue value of the antioxidant containing area. The points were fitted with the Hill Equation in the IGOR data analysis software. To calculate the TEAC, the x_{half} parameter of antioxidants and x_{half} parameter of trolox, as a reference, was compared:

$$\mathrm{TEAC} = \frac{x_{half_{AO}}}{x_{half_{trolox}}}. \quad (6)$$

All measurements were taken three times (n = 3) and the LOD was determined using the following equation:

$$\mathrm{LOD} = \frac{3\delta}{s} \quad (7)$$

where δ is the standard deviation of the control and s is the slope of the fitted line.

Sample preparation for surface enhanced Raman spectroscopy (SERS)

Silver nanoparticles were used to functionalize the filter paper to enhance the Raman intensity, as their size and shape-dependent surface plasmonic properties are widely utilized in SERS experiments.[48] Silver nanoparticles were prepared by the Lee and Meisel method.[49] Accordingly, 500 mL of 1 mM $AgNO_3$ solution was heated to boiling and thereafter, 10 mL of 1% trisodium citrate was added dropwise into the boiling solution under vigorous stirring. The mixture was kept boiling until a green-grey silver colloid was obtained. The dLDH dispersion, the $Cu(Nc)_2$ complex solution and the functionalized dLDH dispersion were uniformly introduced dropwise to the surface of the filter paper. After drying, silver colloid coated filter paper was obtained. The SERS measurements were carried out based on a previously established protocol[50] with a Bruker Senterra II Raman microscope. An excitation wavelength of 532 nm applying 25 mW laser power was used and 128 spectra with an exposition time of 4 s were averaged.

Scanning electron microscopy (SEM)

Morphological analyses of bare and modified filter papers were performed using a Hitachi (Tokyo, Japan) S-4700 SEM at 10 kV accelerating voltage. Small parts of functionalized cellulose paper were cut and glued on the sample holder with double-sided carbon tape. Before the measurement, a gold layer was deposited on the surface of the glued papers.

Results and discussion

Functionalization of dLDH particles

dLDH nanosheets containing Mg^{2+} and Al^{3+} metal ions and charge compensating lactate anions exhibited a uniform size distribution (polydispersity index of 0.176) with a Z-average hydrodynamic size of 47 nm (Fig. S1A†) and a zeta potential of +26.3 mV. The TEM image shows that dLDH has a hexagonal and sheet-like morphology (Fig. S1B†).

Since both dLDH and the $Cu(Nc)_2$ complex have positive surface charge, the direct functionalization of the nanosheets

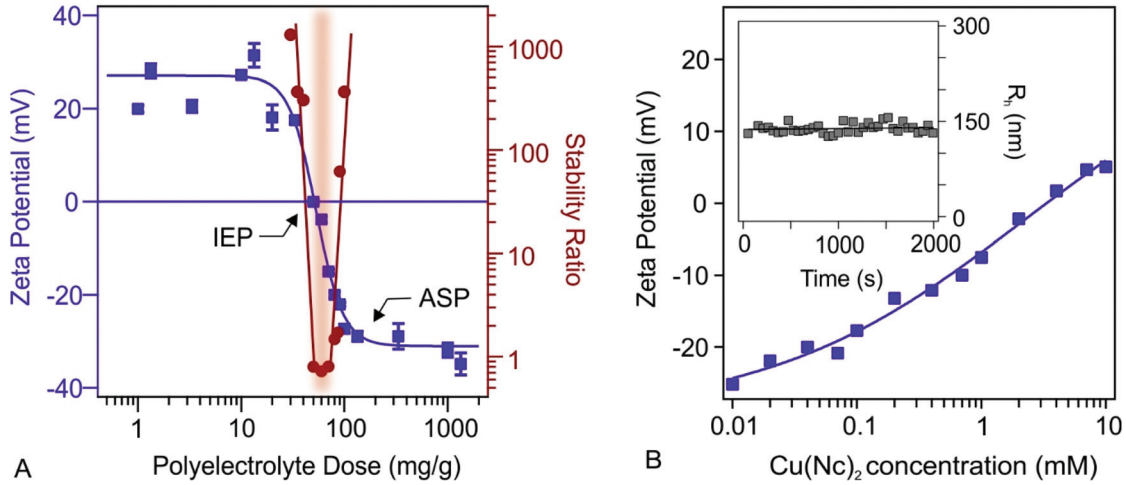

Fig. 1 (A) Zeta potential and stability ratio values at different polyelectrolyte doses. (B) Zeta potentials as a function of the complex concentration. The inset (in B) shows the hydrodynamic radius in time at 0.1 mM Cu(Nc)$_2$ concentration. The solid lines are a guide to the eye. The polyelectrolyte dose in A refers to mg NaAlg per 1 g of dLDH.

with the complex *via* electrostatic interactions is not feasible. Therefore, a negatively charged NaAlg polyelectrolyte was adsorbed on dLDH particles. To optimize the NaAlg dose, zeta potential values were determined at different polyelectrolyte concentrations (Fig. 1A).

At low doses no change can be detected in the zeta potential, while upon increasing the amount of the polyelectrolyte, the potentials decreased. The adsorption of NaAlg on the oppositely charged nanosheets led to charge neutralization at the isoelectric point (IEP at 50 mg g^{-1}), while the surface charge turned negative above this dose. Finally, the zeta potentials decreased until reaching the adsorption saturation plateau (ASP at 150 mg g^{-1}). The particles are fully covered by the polyelectrolytes at the ASP and, thus, further increasing the NaAlg dose gave rise to constant zeta potential values, indicating that the further added NaAlg did not interact with the particle surface. Polyelectrolyte induced charge reversal of surfaces has been already published in the literature and it was related to entropy effects, ion correlations and hydrophobic interactions.[51–53]

The trend in the stability ratios is in good agreement with the zeta potential values if one considers the presence of repulsive forces of electrostatic origin. Accordingly, at low doses, where the particles possess considerable positive charge, aggregation did not occur, *i.e.*, the dispersions were stable. However, at the IEP, where the overall charge is zero, the electrostatic repulsion between the particles vanishes and hence, the particles rapidly aggregate. Note that a stability ratio close to one means that the particles undergo diffusion-controlled aggregation. At higher NaAlg doses, the charge reversal induced the re-entrance of significant surface charges, leading to the rise of repulsive forces stabilizing the samples. These results are further demonstrated by time resolved hydrodynamic radii shown in Fig. S2.† At low and high polyelectrolyte doses the particle size is constant, while close to IEP, hydrodynamic radii increased rapidly.

The above results are in line with the findings reported for other oppositely charged LDH-polyelectrolyte systems.[54] To obtain processable particles of sufficiently high negative charge for Cu(Nc)$_2$ immobilization, 150 mg g^{-1} NaAlg concentration (denoted as dLDH-Alg later) was applied in the further measurements. Under these experimental conditions, the dispersions are stable and the dLDH surface is fully covered with polyelectrolyte chains.

The effects of the possible adsorption processes of Cu(Nc)$_2$ on the charge characteristics of dLDH-Alg were studied *via* zeta potential measurements (Fig. 1B). By increasing the complex concentration, zeta potentials increased, nevertheless, charge reversal occurred to a negligible extent. At low Cu(Nc)$_2$ concentrations, the charge did not change significantly, and thus the dispersions are expected to remain stable. At higher Cu(Nc)$_2$ levels the particle charge was close to zero, which resulted in an unstable dispersion. Therefore, to maintain high colloidal stability, 0.1 mM Cu(Nc)$_2$ concentration was used to functionalize the dLDH-Alg particles (denoted as dLDH-Alg-Cu(Nc)$_2$). Under these complex experimental conditions, particle aggregation was not observed (see the Fig. 1B inset).

Antioxidant tests with bare and immobilized Cu(Nc)$_2$

To prove that the immobilized complexes kept their antioxidant sensing ability, the CuPRAC tests were performed. As mentioned earlier, the assay is based on the redox reaction between Cu(Nc)$_2$ chelate and antioxidant substances (Scheme S1†). During Cu$^+$ formation, the color of the solution shifts from light blue to orange. To evaluate the measurements, the final absorbance values at 450 nm, after 30 minutes of reaction time, were plotted against the initial

antioxidant concentrations (Fig. S3†). The slopes determined from the graphs were compared with the molar absorption coefficient of trolox to calculate TEAC values (see eqn (4)). Once the antioxidant has high efficiency, the color will change more rapidly and the absorbance will increase more significantly. In other words, TEAC values higher than one means that the antioxidant is more efficient than the reference molecule. The TEAC values determined with dLDH-Alg-Cu$(Nc)_2$ and Cu$(Nc)_2$ for ten different antioxidants are shown in Fig. 2.

The aim of these experiments was to compare the sensing capability of the bare and immobilized complex. The data in Fig. 2 indicate that the TEAC values determined by the sensor were similar to the one observed by the complex, while the same trend was observed in the activity of the molecular antioxidants, which can be divided into three groups based on their activity. While ascorbic acid and chlorogenic acid have TEAC values close to one, sodium salicylate, diosmin and glutathione showed lower activity than trolox. However, the rest of the antioxidants (catechin, eugenol, gallic acid and tannic acid) represent higher TEAC values. Note that the complex did not lose the antioxidant sensing ability upon immobilization; therefore, it can be applied as a potential antioxidant sensing element.

Besides, on the basis of the liquid phase CuPRAC measurements using Cu$(Nc)_2$ as a sensing element, a novel single-step method was developed to calculate antioxidant activities without performing experiments at several concentrations. As is shown in Fig. 3, there is a linear relationship between the calculated TEAC and the absorbance values measured at 10 μM concentration of the molecular antioxidants.

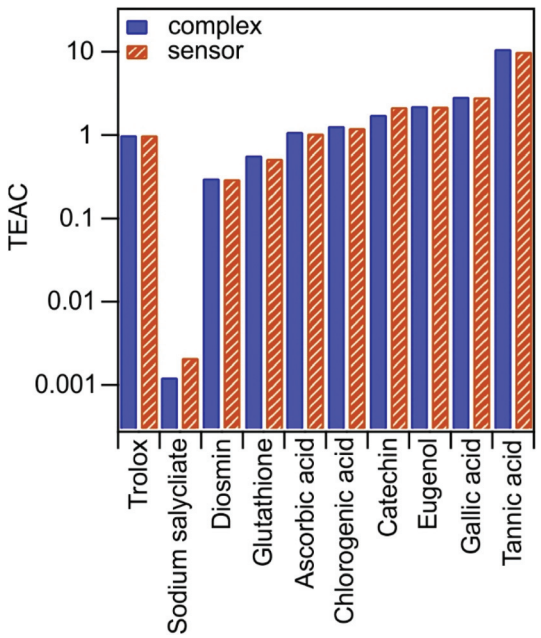

Fig. 2 TEAC values determined by Cu$(Nc)_2$ (complex) and dLDH-Alg-Cu$(Nc)_2$ (sensor) for different molecular antioxidants using eqn (4).

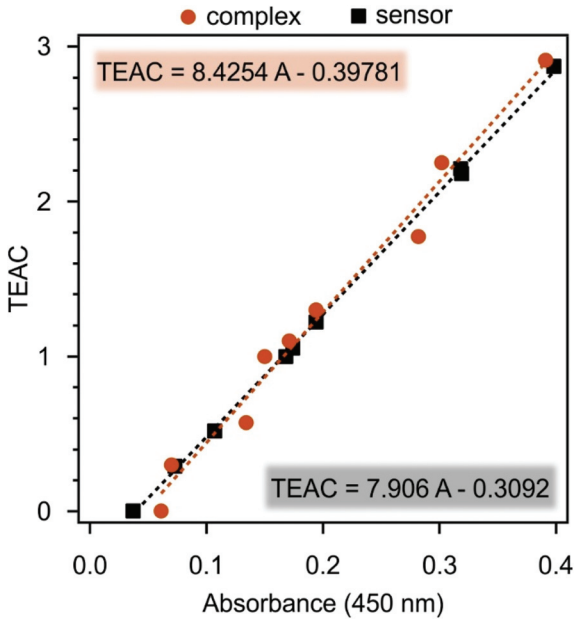

Fig. 3 TEAC values plotted against the absorbance recorded at 450 nm wavelength and 10 μM antioxidant concentration. The dashed lines are linear fits to the data.

By using the parameters obtained from the linear regression of the data, the effectiveness, expressed in TEAC, of the different antioxidants can be determined in a single step. Applying this protocol, the antioxidant activity of substances can be assessed by measuring only one absorbance value and no need for concentration-dependent measurements. This method represents an innovative alternative to replace previously used time consumed protocols to detect antioxidant activity. As another advantage besides faster detection, a much lower sample volume is necessary, since only one experiment is carried out. It is expected that this methodology will be widely applied as a laboratory tool to identify the presence of molecular antioxidants in various samples.

Paper-based sensor

To fabricate an antioxidant sensor, the Cu$(Nc)_2$ complex and the dLDH-Alg-Cu$(Nc)_2$ composite were immobilized on cellulose filter paper surfaces, affording P-Cu$(Nc)_2$ and P-dLDH-Alg-Cu$(Nc)_2$, respectively. First, the presence of Cu$(Nc)_2$ on cellulose filter paper was confirmed by Raman spectroscopy. To increase the Raman signal, silver nanoparticles were attached to the substrate. The Raman spectra of Cu$(Nc)_2$, the paper and P-Cu$(Nc)_2$ are shown in Fig. 4.

The intense peak at around 2900 cm^{-1} indicates CH stretching vibration, while the 1000–1500 cm^{-1} region denotes the C–O–C stretching, HCO and HCC bending vibrations. These bands are characteristic of the cellulose filter paper.[55] In the Raman spectrum of P-Cu$(Nc)_2$ (Fig. 4A(d)), some additional very intense peaks appeared. The vibrational bands found at 1404 cm^{-1} and 1580 cm^{-1} can be related to the C=C stretching mode vibration of the rings in the phenanthroline back-

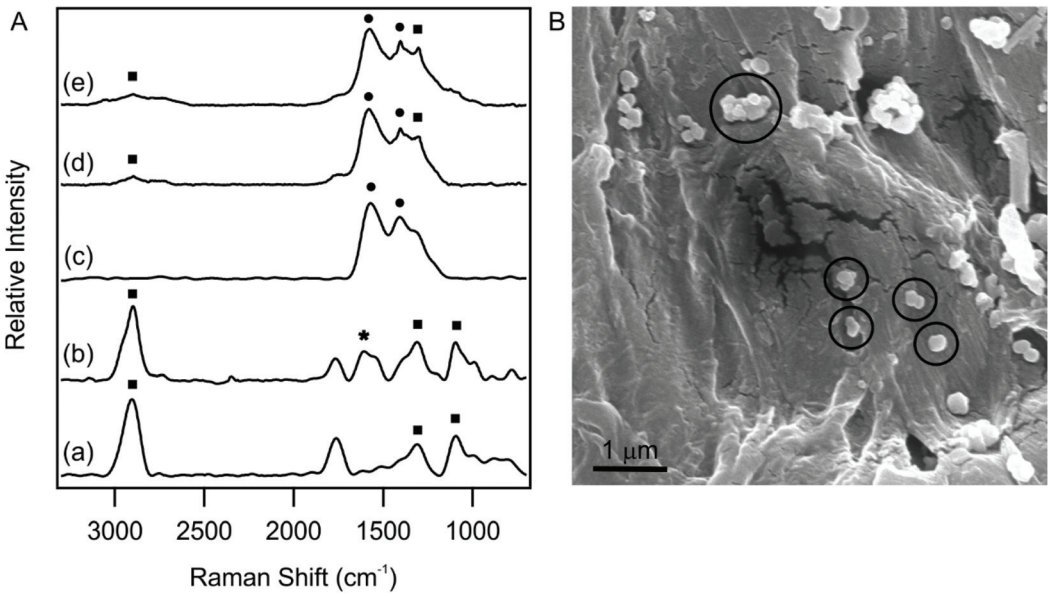

Fig. 4 (A) SERS spectra of cellulose filter paper (a), P-dLDH (b), $Cu(Nc)_2$ (c), P-$Cu(Nc)_2$ (d) and P-dLDH-Alg-$Cu(Nc)_2$ (e). Squares (■) refer to the peaks of the paper substrate, stars (★) for dLDH and circles (●) for $Cu(Nc)_2$. (B) SEM image of P-dLDH-Alg-$Cu(Nc)_2$. The empty circles in (B) indicate the position of dLDH particles.

bone.[56] One of these bands can be found in all $Cu(Nc)_2$, P-Cu $(Nc)_2$ and P-dLDH-Alg-$Cu(Nc)_2$ samples, which unambiguously confirmed the presence of $Cu(Nc)_2$ in each material. The full assignment of the Raman peaks is shown in Table S1.†

SEM analysis confirmed the presence of dLDH particles in the final composite (Fig. 4B). The circles indicate the particles immobilized on the surface. The size of the dLDH particles is in good agreement with the DLS measurements, as the average diameter, calculated from 30 measurements, was found to be (183 ± 30) nm. The SEM images of the paper and the P-$Cu(Nc)_2$ are shown in Fig. S4,† where dLDH particles are not present.

Formulation of sensing elements on paper provides a fast and cheap way to measure the antioxidant activity of different samples. For quantification, the ImageJ software was used in this study, but a portable color reader or a cell phone may be a potential analyzer to detect the antioxidant activity based on color changes. The P-$Cu(Nc)_2$ and P-dLDH-Alg-$Cu(Nc)_2$ without antioxidants were almost colorless. However, a well visible (even to the naked eye) color change occurred immediately after the addition of antioxidant solutions, and it became stronger with the increase of the antioxidant concentration. It was found that the immobilization of the complex on LDH did not affect its sensing reaction towards antioxidants. The photos of paper-based sensors are shown in Fig. S5.† Since the complementary color of orange is blue, blue color intensity values were used to identify the sensor efficiency during the analysis.

For both P-$Cu(Nc)_2$ and P-dLDH-Alg-$Cu(Nc)_2$ the ΔMBV values start to increase upon increasing the antioxidant concentration and after a threshold concentration, the ΔMBV values reach a plateau. The linear increment was fitted (Fig. S6†) and thus, the linear range and LOD values were determined (Table S2 in the ESI†). The linear range values are located in the 3–300 μM range, while the LOD values are under 100 μM in almost every case. With the application of the immobilized complex, the linear range values widened, while the LOD values decreased significantly with a few exceptions. For diosmin and glutathione, the linear range did not broaden but shifted to a somewhat different concentration range. In the case of diosmin, the linearity is shifted to a higher concentration range (150–300 μM), while for glutathione, it is shifted to lower concentration values (80–100 μM). Fig. 5 presents the

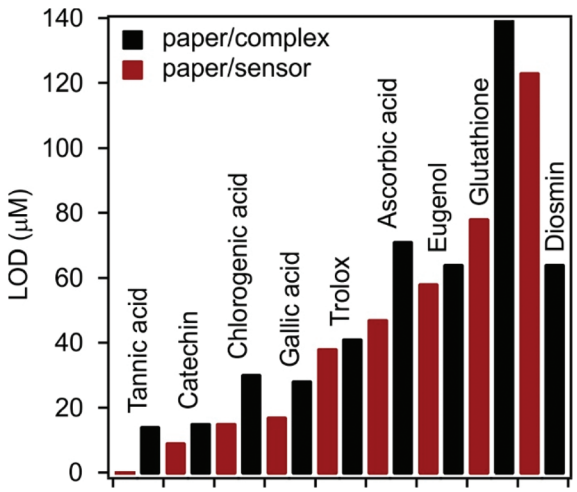

Fig. 5 LOD values determined for the antioxidants by sensor measurements. P-$Cu(Nc)_2$: paper/complex and P-dLDH-Alg-$Cu(Nc)_2$: paper/sensor.

LOD values measured with both P-Cu$(Nc)_2$ and P-dLDH-Alg-Cu$(Nc)_2$.

Accordingly, LOD values were lower with P-dLDH-Alg-Cu$(Nc)_2$ than with P-Cu$(Nc)_2$ for 8 molecular antioxidants, while for diosmin, the opposite trend was observed. The possible reason for the decreased LOD values is that the dLDH particle could not penetrate the paper pores, *i.e.*, they are localized on the surface and thus, they are more capable of interacting with the antioxidant molecules. For catechin, trolox and eugenol, the decrease in the LOD was moderate (less than 10 μM), while for tannic acid, chlorogenic acid and gallic acid LOD values decreased by 14 μM, 15 μM and 11 μM. The most striking improvement in the LOD was in the case of glutathione, with which the LOD difference was 67 μM, when using P-dLDH-Alg-Cu$(Nc)_2$ or P-Cu$(Nc)_2$.

TEAC values were determined based on fitting the experimental data with the Hill equation (Fig. S7†). The tendency in antioxidant detection was similar for Cu$(Nc)_2$ and dLDH-Alg-Cu$(Nc)_2$ (Fig. 2). However, two exceptions were identified. Eugenol exhibited a lower TEAC value, while chlorogenic acid had higher activity during paper-based sensor measurements. Since eugenol has just one active phenolic OH group in its structure (see Table S2†), the loss in activity is possibly due to the formation of H-bonds between the molecules and the cellulose filter paper, covering the active sites. On the other hand, the active groups of chlorogenic acid may be more accessible after interaction with the surface of the sensor than in the liquid phase. The TEAC values determined by the sensor measurements are shown in Table S2,† while the comparison with other methods is collected in Table S3.† The latter data indicate that the sensitivity and the efficiency of P-dLDH-Alg-Cu$(Nc)_2$ is comparable to other sensors reported earlier in the literature. However, its preparation is simpler, *i.e.*, synthesis of dLDH is facile and cheap as well as no need for using complicated sensor elements such as membranes or electrodes.

Conclusion

Mobile, on-site measurements demand the continuous development of sensors to assess their qualities and quantities in a rapid fashion. Herein, a paper-based sensor was developed for the facile detection of molecular antioxidants. NaAlg functionalized dLDH nanosheets were used as carriers for the immobilization of Cu$(Nc)_2$, which was applied as the color changing center. It was found that the optimal conditions for the sensor preparation required a magnitude lower Cu$(Nc)_2$ concentration compared to the traditional CuPRAC method. The prepared composite was placed on cellulose paper as a stable and homogenous suspension followed by fixation by drying. SERS confirmed the presence of characteristic vibration bands of chelating neocuproine on the sensor, while the platelets of dLDH were spotted on SEM micrographs. The sensitivity and linearity of antioxidant detection were also determined. Ten molecular antioxidants were under investigation and color change accompanying the reduction of Cu$(Nc)_2$ was more intensive with a higher concentration of the antioxidant, *i.e.*, the reaction was as sensitive to the presence of antioxidants as the traditional cuvette method. The linearity ranges determined with P-dLDH-Alg-Cu$(Nc)_2$ were compared to the ones measured with P-Cu$(Nc)_2$ and an evident range expansion was pointed out in the majority of the systems. This enables the sensor to be applied at wider concentration ranges, while the LOD values also shifted to lower antioxidant concentrations. In conclusion, a sensor with the ease of preparation was developed for the evaluation of the antioxidant efficiency with a facile color intensity measurement, offering a potential upgrade for portable colorimetric or cell phone analysis.

Conflicts of interest

There are no conflicts to declare.

Acknowledgements

The research was financially supported by the Eötvös Lóránd Research Network through the Lendület Program (96130) and by project no. TKP2021-NVA-19, which has been implemented with the support provided by the Ministry of Innovation and Technology of Hungary from the National Research, Development and Innovation Fund, financed under the TKP2021-NVA funding scheme. SM acknowledges the support from the Ministry of Human Capacities of Hungary (NTP-NFTÖ-20-B-0035). The support from the University of Szeged Open Access Fund (5662) is gratefully acknowledged.

References

1 C. C. Winterbourn, *Nat. Chem. Biol.*, 2008, **4**, 278–286.
2 S. B. Nimse and D. Pal, *RSC Adv.*, 2015, **5**, 27986–28006.
3 K. M. Gupta, S. Das, P. S. Chow and C. Macbeath, *ACS Appl. Nano Mater.*, 2020, **3**, 5351–5361.
4 J. Bouayed and T. Bohn, *Oxid. Med. Cell. Longevity*, 2010, **3**, 228–237.
5 S. Ahmed, S. A. Sulaiman, A. A. Baig, M. Ibrahim, S. Liaqat, S. Fatima, S. Jabeen, N. Shamim and N. H. Othman, *Oxid. Med. Cell. Longevity*, 2018, 8367846, DOI: 10.1155/2018/8367846.
6 C. Nirmala, M. S. Bisht, H. K. Bajwa and O. Santosh, *Trends Food Sci. Technol.*, 2018, **77**, 91–99.
7 S. C. Lourenco, M. Moldao-Martins and V. D. Alves, *Molecules*, 2019, **24**, 4132.
8 F. Karimi, E. Shaabani, I. Martinez-Rovira, I. Yousef, M. H. Ghahremani and S. Kharrazi, *Analyst*, 2021, **146**, 6902–6916.
9 Y. H. Lin, Y. P. Chen, T. P. Liu, F. C. Chien, C. M. Chou, C. T. Chen and C. Y. Mou, *ACS Appl. Mater. Interfaces*, 2016, **8**, 17944–17954.
10 T. J. Gutierrez, A. G. Ponce and V. A. Alvarez, *Mater. Chem. Phys.*, 2017, **194**, 283–292.

11 A. M. Pudlarz, E. Czechowska, M. S. Karbownik, K. Ranoszek-Soliwoda, E. Tomaszewska, G. Celichowski, J. Grobelny, E. Chabielska, A. Gromotowicz-Poplawska and J. Szemraj, *Nanomedicine*, 2020, **15**, 23–39.
12 J. Hari, A. Gyurki, M. Sarkozi, E. Foldes and B. Pukanszky, *J. Colloid Interface Sci.*, 2016, **462**, 123–129.
13 S. Murath, S. Szerlauth, D. Sebok and I. Szilagyi, *Antioxidants*, 2020, **9**, 153.
14 T. Katsube, H. Tabata, Y. Ohta, Y. Yamasaki, E. Anuurad, K. Shiwaku and Y. Yamane, *J. Agric. Food Chem.*, 2004, **52**, 2391–2396.
15 A. Senocak, E. Korkmaz, A. Khataee and E. Demirbas, *Mater. Chem. Phys.*, 2022, **275**, 125298.
16 M. Bener, M. Ozyurek, K. Guclu and R. Apak, *Anal. Chem.*, 2010, **82**, 4252–4258.
17 A. Cardenas and C. Frontana, *Sens. Actuators, B*, 2020, **313**, 128070.
18 W. Brand-Williams, M. E. Cuvelier and C. Berset, *LWT–Food Sci. Technol.*, 1995, **28**, 25–30.
19 I. F. F. Benzie and J. J. Strain, *Anal. Biochem.*, 1996, **239**, 70–76.
20 R. Re, N. Pellegrini, A. Proteggente, A. Pannala, M. Yang and C. Rice-Evans, *Free Radicals Biol. Med.*, 1999, **26**, 1231–1237.
21 R. Apak, K. Guclu, M. Ozyurek and S. E. Karademir, *J. Agric. Food Chem.*, 2004, **52**, 7970–7981.
22 F. Y. Tian, R. J. Fu, J. Zhou, Y. L. Cui, Y. H. Zhang, B. N. Jiao and Y. He, *Sens. Actuators, B*, 2020, **321**, 128604.
23 M. Bener and R. Apak, *Sens. Actuators, B*, 2017, **247**, 155–162.
24 Y. Vlamidis, I. Gualandi and D. Tonelli, *J. Electroanal. Chem.*, 2017, **799**, 285–292.
25 A. Casanova, M. Cuartero, Y. Alacid, C. M. Almagro, F. Garcia-Canovas, M. S. Garcia and J. A. Ortuno, *Analyst*, 2020, **145**, 3645–3655.
26 A. Othman, L. Norton, A. S. Finny and S. Andreescu, *Talanta*, 2020, **208**, 120473.
27 F. Della Pelle and D. Compagnone, *Sensors*, 2018, **18**, 462.
28 Y. Wang, P. Zhang, W. S. Fu and Y. N. Zhao, *Biosens. Bioelectron.*, 2018, **122**, 183–188.
29 C. Puangbanlang, K. Sirivibulkovit, D. Nacapricha and Y. Sameenoi, *Talanta*, 2019, **198**, 542–549.
30 G. A. Crespo, M. G. Afshar and E. Bakker, *Angew. Chem., Int. Ed.*, 2012, **51**, 12575–12578.
31 X. J. Xie, G. Mistlberger and E. Bakker, *J. Am. Chem. Soc.*, 2012, **134**, 16929–16932.
32 G. Mistlberger, X. J. Xie, M. Pawlak, G. A. Crespo and E. Bakker, *Anal. Chem.*, 2013, **85**, 2983–2990.
33 V. V. Apyari, V. V. Arkhipova, M. V. Gorbunova, P. A. Volkov, A. I. Isachenko, S. G. Dmitrienko and Y. A. Zolotov, *Talanta*, 2016, **161**, 780–788.
34 Q. Wang and D. O'Hare, *Chem. Rev.*, 2012, **112**, 4124–4155.
35 S. Murai, Y. Tokudome, R. Katsura, H. Sakamoto, K. Noguchi, M. Takahashi and K. Tanaka, *ACS Appl. Nano Mater.*, 2020, **3**, 5838–5845.
36 C. Martini, C. Ferroni, M. B. Gariboldi, A. Donnadio, A. Aluigi, G. Sotgiu, F. Liscio, P. Dambruoso, M. L. Navacchia, T. Posati and G. Varchi, *ACS Appl. Nano Mater.*, 2018, **1**, 6387–6397.
37 Y. Yao, M. L. Xue, W. Mao, Y. N. Li, A. N. Zhu, T. Y. Chen, W. Shen, C. Liu, L. Z. Chen and S. Tang, *Analyst*, 2021, **146**, 6470–6473.
38 M. Konari, E. Heydari-Bafrooei and M. Dinari, *Int. J. Biol. Macromol.*, 2021, **166**, 54–60.
39 S. J. Yang, M. Y. Liu, F. J. Deng, L. C. Mao, S. X. Yu, H. Y. Huang, J. Y. Chen, L. J. Liu, X. Y. Zhang and Y. Wei, *Colloid Interface Sci. Commun.*, 2020, **37**, 100294.
40 Y. L. Wang, Z. C. Wang, Y. P. Rui and M. G. Li, *Biosens. Bioelectron.*, 2015, **64**, 57–62.
41 Y. W. Zhang, J. Q. Tian, S. Liu, L. Wang, X. Y. Qin, W. B. Lu, G. H. Chang, Y. L. Luo, A. M. Asiri, A. O. Al-Youbi and X. P. Sun, *Analyst*, 2012, **137**, 1325–1328.
42 L. Li, Z. Gu, W. Y. Gu and Z. P. Xu, *RSC Adv.*, 2016, **6**, 95518–95526.
43 A. V. Delgado, E. Gonzalez-Caballero, R. J. Hunter, L. K. Koopal and J. Lyklema, *Pure Appl. Chem.*, 2005, **77**, 1753–1805.
44 P. A. Hassan, S. Rana and G. Verma, *Langmuir*, 2015, **31**, 3–12.
45 G. Trefalt, I. Szilagyi, T. Oncsik, A. Sadeghpour and M. Borkovec, *Chimia*, 2013, **67**, 772–776.
46 H. Holthoff, S. U. Egelhaaf, M. Borkovec, P. Schurtenberger and H. Sticher, *Langmuir*, 1996, **12**, 5541–5549.
47 M. Ozyurek, K. Guclu, E. Tutem, K. S. Baskan, E. Ercag, S. E. Celik, S. Baki, L. Yildiz, S. Karaman and R. Apak, *Anal. Methods*, 2011, **3**, 2439–2453.
48 M. Moskovits, *Rev. Mod. Phys.*, 1985, **57**, 783–826.
49 P. C. Lee and D. Meisel, *J. Phys. Chem.*, 1982, **86**, 3391–3395.
50 Z. Q. Niu and Y. Fang, *J. Colloid Interface Sci.*, 2006, **303**, 224–228.
51 M. Quesada-Perez, E. Gonzalez-Tovar, A. Martin-Molina, M. Lozada-Cassou and R. Hidalgo-Alvarez, *ChemPhysChem*, 2003, **4**, 235–248.
52 J. Lyklema, *Colloids Surf., A*, 2006, **291**, 3–12.
53 Q. H. Chang and J. Jiang, *Macromolecules*, 2021, **54**, 4145–4153.
54 M. Pavlovic, P. Rouster, T. Oncsik and I. Szilagyi, *ChemPlusChem*, 2017, **82**, 121–131.
55 J. H. Wiley and R. H. Atalla, *Carbohydr. Res.*, 1987, **160**, 113–129.
56 N. H. Jang, J. S. Suh and M. Moskovits, *J. Phys. Chem. B*, 1997, **101**, 8279–8285.